The Astrophysical Journal, 829:91 (7pp), 2016 October 1 doi:10.3847/0004-637X/829/2/91

EVIDENCE OF SPREADING LAYER EMISSION IN A THERMONUCLEAR SUPERBURST

K. I. I. Koljonen[1], J. J. E. Kajava[2], and E. Kuulkers[2]
[1] New York University Abu Dhabi, P.O. Box 129188, Abu Dhabi, UAE; karri.koljonen@nyu.edu
[2] European Space Astronomy Centre (ESA/ESAC), Science Operations Department, E-28691, Villanueva de la Cañada, Madrid, Spain
Received 2016 April 27; accepted 2016 June 1; published 2016 September 26

ABSTRACT

When a neutron star (NS) accretes matter from a companion star in a low-mass X-ray binary, the accreted gas settles onto the stellar surface through a boundary/spreading layer. On rare occasions the accumulated gas undergoes a powerful thermonuclear superburst powered by carbon burning deep below the NS atmosphere. In this paper, we apply the non-negative matrix factorization spectral decomposition technique to show that the spectral variations during a superburst from 4U 1636–536 can be explained by two distinct components: (1) the superburst emission characterized by a variable temperature blackbody radiation component and (2) a quasi-Planckian component with a constant, ∼2.5 keV, temperature varying by a factor of ∼15 in flux. The spectrum of the quasi-Planckian component is identical in shape and characteristics to the frequency-resolved spectra observed in the accretion/persistent spectrum of NS low-mass X-ray binaries and agrees well with the predictions of the spreading layer model by Inogamov & Sunyaev. Our results provide yet more observational evidence that superbursts—and possibly also normal X-ray bursts—induce changes in the disc–star boundary.

Key words: accretion, accretion disks – stars: neutron – X-rays: bursts

1. INTRODUCTION

Low-mass stars in interacting binary configurations with a neutron star (NS) are the most common type among low-mass X-ray binaries (LMXB; see, e.g., Tauris & van den Heuvel 2006, pp. 623–665; Done et al. 2007, for a review). The mass lost by the low-mass star is accumulated onto the NS surface through an accretion disc. In order for the matter to decelerate from Keplerian disk rotation to the slower rotational motion of the NS, a boundary layer (BL) must form between the accretion disk and the NS surface. The energy release in this process is substantial and the resulting radiation from the BL can be more luminous than the radiation from the accretion disk (Sunyaev & Shakura 1986). The physical properties, the geometry, and the radiation mechanisms of such BLs are not well known at present. Moreover, depending on the accretion state of the NS–LMXB, the properties and radiation mechanism of the BL can be different. In the hard ("island") spectral state, the optically thick accretion disk may be truncated to larger radii (Done et al. 2007) and the optically thin, hot inner flow smoothly connects to the NS through an optically thin BL (Deufel et al. 2001). When the accretion rate increases, the inner edge of the disk moves inwards and the hot, inner flow collapses/condensates into the disk (e.g., Meyer et al. 2007). As the source moves from the hard state to the soft ("banana") spectral state, the BL becomes optically thick to Comptonization and cools down causing a rapid drop in the X-ray hardness ratio (Done et al. 2007). Two distinct geometries of the BL are considered possible. In a classical BL model, the rotational velocity decreases over a large radial extent in the disc midplane (e.g., Pringle 1977; Sunyaev & Shakura 1986; Popham & Sunyaev 2001), or in the alternative spreading layer (SL) model the radial extent of the layer is smaller but the gas spreads over a considerable height from the equatorial plane toward higher stellar latitudes (e.g., Inogamov & Sunyaev 1999, 2010). Radiative transfer calculations of the BL model by Grebenev & Sunyaev (2002) predict spectra that are harder than those observed in NS–LMXBs in the soft spectral state, whereas the SL model calculations by Suleimanov & Poutanen (2006) predict softer, quasi-Planckian spectra with a color temperature of 2.4–2.6 keV, as long as the accretion rate ($\dot{M}$) is sufficiently high (>10% of the Eddington accretion rate). The SL model predictions are in good agreement with observed values of NS–LMXBs in the soft spectral state (e.g., Mitsuda et al. 1984; Lin et al. 2007).

During accretion episodes NS–LMXBs may show "superbursts," which are rare and unusually long thermonuclear X-ray bursts (Cornelisse et al. 2000). Superbursts last several hours whereas the much more commonly observed type-I X-ray bursts (see Lewin et al. 1993 for review) last only 10–100 s. This difference is thought to arise from different burning regimes in the NS atmosphere. The type-I X-ray bursts are powered by helium and/or hydrogen burning in the NS "ocean," while the superbursts are powered by carbon burning at greater depths (Cumming & Bildsten 2001). To date, only a handful of superbursts have been observed, with only two that have high quality data covering most of the burst: 4U 1636–536 (Strohmayer & Markwardt 2002) and 4U 1820–303 (Strohmayer & Brown 2002). During a thermonuclear burst the X-ray emission in NS–LMXBs can arise from three distinct regions that are all emitting more or less in the same energy band with similar spectral shapes: an X-ray bursting NS surface, a BL/SL, and an accretion disc. During an X-ray burst the NS surface can heat up to 3 keV, radiating blackbody-like emission with temperatures comparable to that of the BL/SL. If the source is in the soft X-ray spectral state, the accretion disc radiates as a multicolor blackbody with a temperature of ∼1 keV, in addition to acting as a reflecting medium for the emission from the bursting NS surface and the BL/SL (Ballantyne 2004). Observationally, the typical NS–LMXB spectrum in the soft state and/or during an X-ray burst is smooth and curved, and can be fitted with several models that include multiple blackbody-like components with varying temperatures. Usually, the models are degenerate so that the source spectra cannot be fitted unambiguously with a single model, but rather with a variety of models with a comparable fit quality (Lin et al. 2007). Thus, this ambiguity

can lead to a completely different physical interpretations depending on the choice of model.

In the past, there have been attempts to overcome this ambiguity by using extra information from the timing domain to decompose the constituent components forming the total spectra, first in Mitsuda et al. (1984), and subsequently in Gilfanov et al. (2003), Revnivtsev & Gilfanov (2006), and Revnivtsev et al. (2013). By using frequency-resolved energy spectra they were able to show that the flux variations on timescales of less than a second are caused by a spectral component of a constant spectral shape varying in normalization. In all of the NS–LMXBs studied, the spectral shape of this component was similar and represented the emission from the SL. Similar ambiguities arise when modeling the X-ray spectra of superbursts. For example, Keek et al. (2014a, 2014b, 2015) used reflection models, in addition to the variable background method (Worpel et al. 2013; in't Zand et al. 2013), in fitting the spectra from the 4U 1636–536 superburst. The persistent emission was seen to vary significantly during the superburst, which was interpreted to be caused by an increase of the mass accretion rate due to Poynting–Robertson drag. Here, the traditional spectral modeling approach left ambiguities as to whether the persistent spectrum changed only in flux, or if the persistent spectral shape was also variable during the superburst.

In this paper, we extend the above-mentioned spectral decomposition studies to include a thermonuclear superburst from 4U 1636–536, and instead concentrate on slower time variability (16 s). By using spectral decomposition methods described in Koljonen (2015), we show that during the superburst a component identical to the SL seen in the persistent emission can be found to contribute a sizable fraction of the total luminosity. Smoothly evolving emission from the SL naturally explains the light curves and spectral evolution of the superburst.

2. OBSERVATIONS AND METHODS

We used data from the Proportional Counter Array (PCA; Jahoda et al. 2006) onboard the *Rossi X-ray Timing Explorer* (*RXTE*) taken during the superburst from 4U 1636–536 (Strohmayer & Markwardt 2002) on 2002 February 22. We extracted the Standard 2 PCA spectra from observation IDs 50030-02-08-01 and 50030-02-08-02, at intervals of 16 s using HEASOFT 6.17. We used PCUs 0, 2, and 3 and extracted spectra from all three detector layers. The exposure times were corrected for deadtime effects, and we used one background and response per orbit produced by the tools PCABACKEST and PCARSP, respectively. The spectra were restricted to span the 3–18 keV range to ensure positive values in all channels throughout the superburst for the decomposition procedure, but for the spectral fitting we used a slightly wider band of 3–20 keV. The fitting was conducted using ISIS (Houck & Denicola 2000), and 0.5% systematic error was introduced to the PCA data. The errors of the resulting fit parameters are quoted at the 90% confidence level.

2.1. Spectral Decomposition

Unsupervised spectral decomposition methods have been proven to be a powerful tool in separating a set of X-ray spectra from X-ray binaries and active galactic nuclei into subcomponents (Vaughan & Fabian 2004; Malzac et al. 2006; Koljonen et al. 2013; Koljonen 2015; Parker et al. 2015; Degenaar et al. 2016). In general, the X-ray spectra are decomposed to their constituent components by using matrix factorization techniques, e.g., principal component analysis. In these techniques a source matrix, X_{ji}, consisting of a discrete set of spectra with flux values for each energy j and each spectrum i, can be linearly decomposed to a mixture of separate source signals S_{ki} weighted over the energy bands by a weight matrix W_{jk} in such a way that $X_{ij} \approx \sum_k W_{jk} S_{ki}$, where k is a dummy variable denoting the running number of components in the decomposition. Usually, the number k is small, and only a few components are needed to explain the variability in the data set within data errors. In practice, we can think the weights of a single component as its spectral shape, which has a variable amplitude denoted by the corresponding signal.

In this paper, we use non-negative matrix factorization (NMF; Paatero & Tapper 1994; Lee & Seung 1999) to decompose the data from the thermonuclear superburst of 4U 1636–536. NMF was found to perform the best of a collection of linear decomposition methods in disentangling different spectral components in simulated X-ray spectra (Koljonen 2015). As spectral evolution typically contains nonlinear effects in LMXBs, such as the changing temperature of the blackbody radiation, this will cause the NMF to estimate this effect as a collection of multiple linear components. However, by summing these components together, we are able to estimate the nonlinearity present in the spectra (see the simulation studies in Koljonen 2015). In the following, the NMF technique is briefly described, and the reader is referred to Koljonen (2015) for more detailed discussion.

In NMF, the matrices W and S are found by minimizing a cost function (generalized Kullback–Leibler divergence) under the constraint that they must be non-negative. For calculating the decomposition we used the package NMF (Gaujoux & Seoighe 2010) that calculates the standard NMF (Brunet et al. 2004) by picking random starting values for W and S from a uniform distribution [0, max(X)] and then updating iteratively 10000 times to find a local minimum of the cost function with a multiplicative rule from Lee & Seung (2001). The minimization process is repeated for 300 starting points to ensure that the algorithm does not get stuck in a local minimum. Despite this, we found that the solutions have a certain amount of scatter in the resulting NMF components and thus we ran the analysis several times to probe the effect of this scatter (see below).

To determine the degree of factorization, k, we use the χ^2-diagram method devised in Koljonen (2015). In general, we expect the quality of the factorization, i.e., its similarity with the original data, to be an increasing function of k. We aim for a value of k which provides substantially better approximation than nearby smaller values, but only a slightly worse approximation than nearby larger values. In the χ^2-diagram method, the reduced χ^2-values are calculated between each individual spectrum in the data set with associated errors and the factorization $\sum_k W_{jk} S_{ki}$. Then a median is taken from all the χ^2-values for a particular k:

$$\chi^2_{\mathrm{red}}(k) = \mathrm{Mdn}\left\{\frac{\sum_i \left[(X_{ji} - \sum_k W_{jk} S_{ki})/\sigma_{ji}\right]^2}{\max(j) - k}\right\}. \quad (1)$$

This produces a quality measure of how well a particular factorization with a degree k fits in to the data and takes into

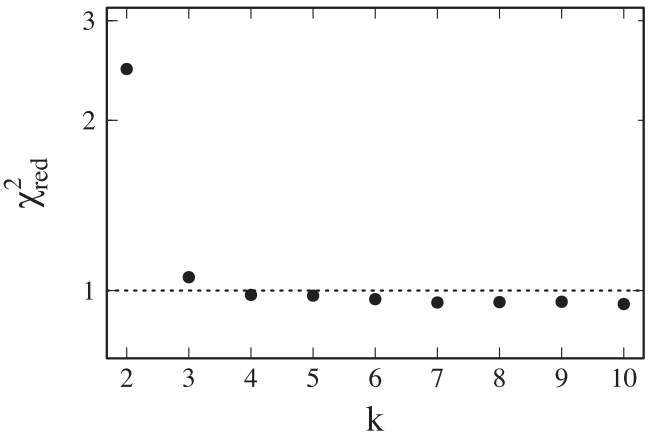

Figure 1. Determining the degree of factorization for NMF analysis. The figure shows the χ^2-diagram of the superburst data set from 4U 1636–536. After $k = 3$, the χ^2-diagram achieves a value where further increasing the degree of factorization reduces the χ^2_{red}-value only by a small amount (i.e., a kink or an elbow in the diagram). Three components are enough to explain the spectral variability of 4U 1636–536 during the superburst.

account the number of components up to those that vary above the noise level.

3. RESULTS

3.1. NMF Components

We begin by calculating the χ^2-diagram for the superburst data set of 4U 1636–536 (Figure 1). As mentioned above, the chosen degree of factorization should be a point where the quality measure changes from steep to shallow (i.e., a kink or an elbow in the diagram). In addition, this value should be close to 1, so that the decomposition would portray faithfully the original spectra. We identify that three components are enough to explain the variability in the data during the superburst.

Figure 2 shows the signals and weights of one NMF run for three components. The smaller upper panels show the source signals S_{ki} and the bottom panels the weights W_{jk}. Note that the ordering of the NMF components is random and does not portray any information. The $k = 1$ most likely represents the emission component from the SL, and the other components are likely caused by the cooling burst spectra. As the NMF relies on linear decomposition, it is best suited for finding the variability of a spectral component that varies in normalization. As mentioned above, the nonlinear effects can be estimated by summing two or more components together that form the spectral component presenting nonlinear behavior; in this case the cooling burst spectrum.

We ran the NMF analysis 200 times to look for deviations in the solutions of the decomposition. Figure 3 shows the weights of the resulting NMF components. We note that some amount of scatter is present in the weights of individual NMF runs. However, the weights across the different energy bands, i.e., the "shape of the spectrum," are fairly consistent in all of the runs. Thus, there exists a small amount of ambiguity in the individual NMF solutions which we take into account in the analysis below.

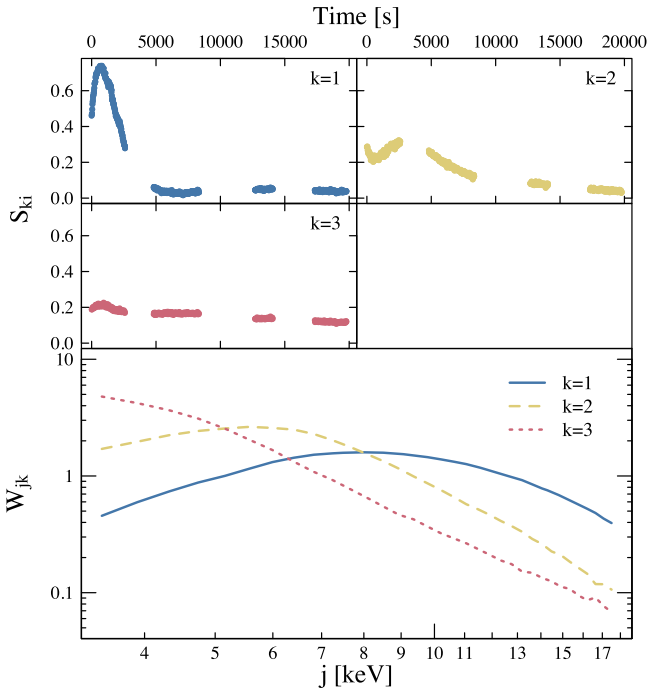

Figure 2. The three NMF components that explain most of the spectral variability in the 4U 1636–536 superburst data set. The smaller top panels show the source signals S_{ki}, and larger bottom panel the weights W_{jk} of the decomposition. The $k = 1$ component likely represents the SL.

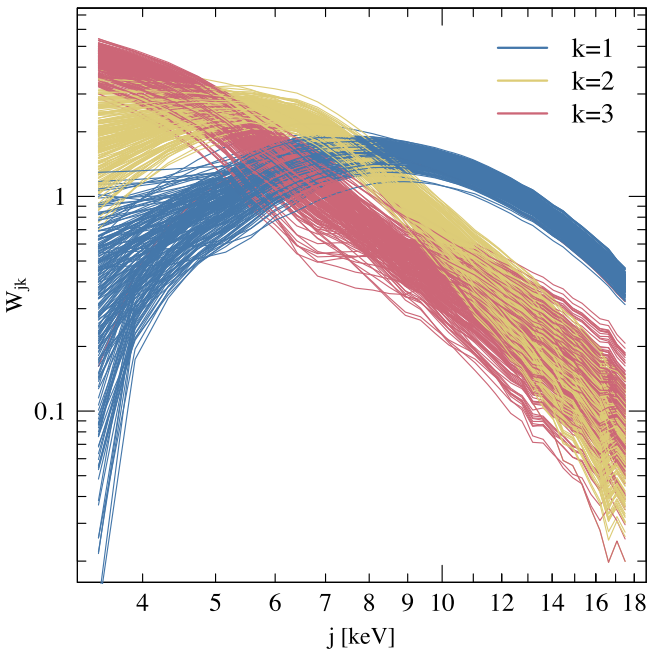

Figure 3. A sample of weights from multiple NMF runs on the superburst data set of 4U 1636–536. The weights vary slightly from run to run, but the overall shape is retained.

3.2. Spectral Components

To interpret the NMF components, we start by reconstructing spectral components from the NMF components we propose as representing the SL ($k = 1$) and the cooling burst ($k = 2,\ 3$). This can be done simply by combining the calculated weight matrix and signal to form the constructed

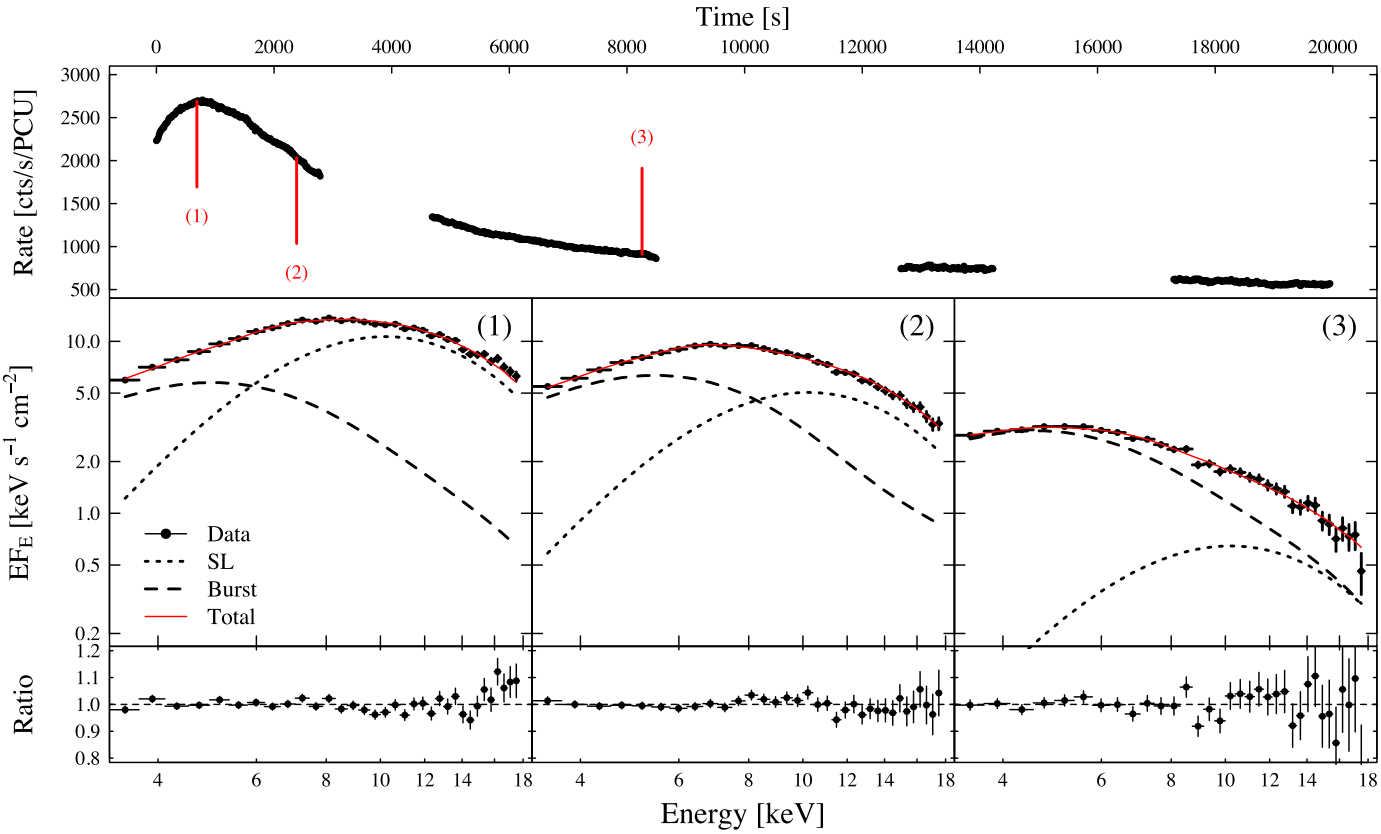

Figure 4. *RXTE*/PCA lightcurve from the 2002 February 22 superburst of 4U 1636-536 (top panel). Selected spectra from three parts of the superburst decomposed to their corresponding NMF components (middle panels). The ratio of the selected spectra and the NMF decomposition (bottom panels).

SL spectra as $M_{\rm SL} = W_{jk} S_{ki}$, where $k = 1$, and for the burst spectra as $M_{\rm B} = \sum_k W_{jk} S_{ki}$, where $k = 2, 3$. In Figure 4, we show three spectra along the superburst (~700 s, 2400 s, and 8200 s after the start of the burst; top panel), together with their decomposition to $M_{\rm SL}$ and $M_{\rm B}$ corresponding to the NMF run shown in Figure 2. During the peak of the superburst (left, middle panel), the SL component dominates the total spectrum, but around 2000 s after the start of the burst (center panel) both components contribute roughly the same amount to the total spectrum and from there on the burst component starts to dominate the total spectrum (right, middle panel).

For each NMF run, we construct the $M_{\rm SL}$ and $M_{\rm B}$, and calculate the average spectra, $\bar{M}_{\rm SL}$ and $\bar{M}_{\rm B}$, out of all runs. The errors for the averaged spectra are estimated as a square root of the unbiased sample variance: $\sigma^2 = 1/(n-1) \sum_{i=1}^{n} (M_i - \bar{M})^2$. These spectra are then imported to ISIS for spectral fitting.

For the averaged SL spectrum, we found that above 6 keV it is well-fitted with a blackbody model (BBODYRAD) with a temperature of 2.56 keV, but at lower energies the SL spectrum is underluminous, similar to the more detailed calculation of the spectrum from SL by Suleimanov & Poutanen (2006). A better fit is obtained when using a saturated Comptonization model (COMPTT; Titarchuk 1994) with the temperature of the seed photons $kT_{\rm s} = 1.5 \pm 0.2$ keV, and the temperature of the Comptonizing electrons $kT_{\rm e} = 2.56 \pm 0.05$ keV, while fixing the optical depth to $\tau = 20$. The fit is not very sensitive to a particular value of τ as long as it is fairly high, i.e., optically thick. Figure 5 shows the difference between the blackbody and the Comptonization model as fitted to the averaged SL spectrum taken from the peak of the superburst. Similarly, in Revnivtsev et al. (2013) the frequency-resolved energy spectrum from the SL component was found to be well-fitted with a saturated Comptonization model.

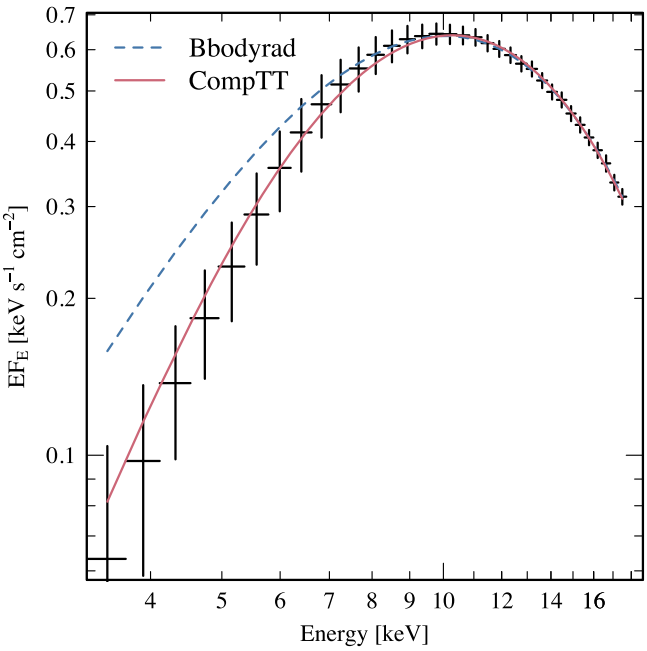

Figure 5. SL spectrum from 4U 1636–536 fitted with the best-fit saturated Comptonization model (solid red line) and blackbody radiation model as fitted to the data over 6 keV (dashed blue line). Both models converge over 10 keV but deviate at lower energies.

For the averaged burst spectrum, we found that it can be fitted with a cooling blackbody model (BBODYRAD) with an additional spectral component in the higher energies. This component can be modeled with a power law, but also the above SL model result in equally good fits. If the SL spectral component varies in concert with the burst spectra, it is possible that it has partly "leaked" to the burst spectra.

3.3. Spectral Fitting

In order to self-consistently verify the NMF decomposition and the above spectral model, we fit the original data with the model PHABS × (COMPTT + BBODYRAD). The parameters of the COMPTT component are fixed to the values mentioned above, with the normalization left free. The absorption column density is fixed to 0.38×10^{22} cm^{-2} (Pandel et al. 2008). Thus, this leaves three free parameters in the model: the normalizations of the blackbody and Comptonization components, and the temperature of the blackbody radiation, i.e., these can be thought as three degrees of freedom mirroring the NMF result that three components are enough to explain most of the spectral variability. The evolution of these parameters and corresponding fluxes throughout the superburst are displayed in Figure 6. The top panel shows the unabsorbed, bolometric (0.1–100 keV) fluxes from the blackbody (BB) and Comptonization (SL) components together with the total bolometric flux (TOT). The middle panels show the apparent blackbody radius at 6 kpc (Galloway et al. 2006) calculated from the blackbody normalization, the temperature of the blackbody, and the normalization of the COMPTT model, respectively. The bottom panel shows the reduced χ^2 values of the spectral fits. The flux from the SL component decreases by a factor of ∼15 during the superburst and at its brightest contributes more than 60% of the total flux. The blackbody flux (mirroring the evolution of the blackbody temperature) is fairly constant at the peak of the burst exhibiting a small dip, and then decreases by a factor of 3 as the burst cools from ∼1.4 keV to ∼1.0 keV. During the superburst the effective NS radius stays at a fairly constant value of ∼12 km, but during the burst decay a clear trend can be seen where the radius increases from 11 to 13 km.

Previous studies have shown (Keek et al. 2014a, 2014b) that the burst spectrum is accompanied by iron features in the form of an iron line around 6.5 keV and an iron edge (or a blend of iron edges) around 9 keV. We found that the 16 s resolution data does not prominently show line or edge features, and we can adequately fit all spectra with the above model. However, the fit residuals (Figure 7) show features around the 4–10 keV energy range that are likely caused by the iron features. In this paper, we are more interested in the continuum components, and thus we leave the detailed spectral modeling to a future publication (J. J. E. Kajava et al. 2016, in preparation).

Finally, we compare the blackbody and SL component fluxes to their corresponding NMF signals. Figure 8 shows the averaged signals from the NMF runs plotted against the component fluxes from the spectral analysis. A linear relation is evident with slight deviations either from our use of a simple spectral model, component leaking in the NMF as discussed above, or that some (small) spectral features are not represented by the three NMF components (the $\chi^2_{\rm red}$ is lower at $k = 4$, see Figure 1). Thus, we can state that the spectral modeling agrees with the NMF analysis.

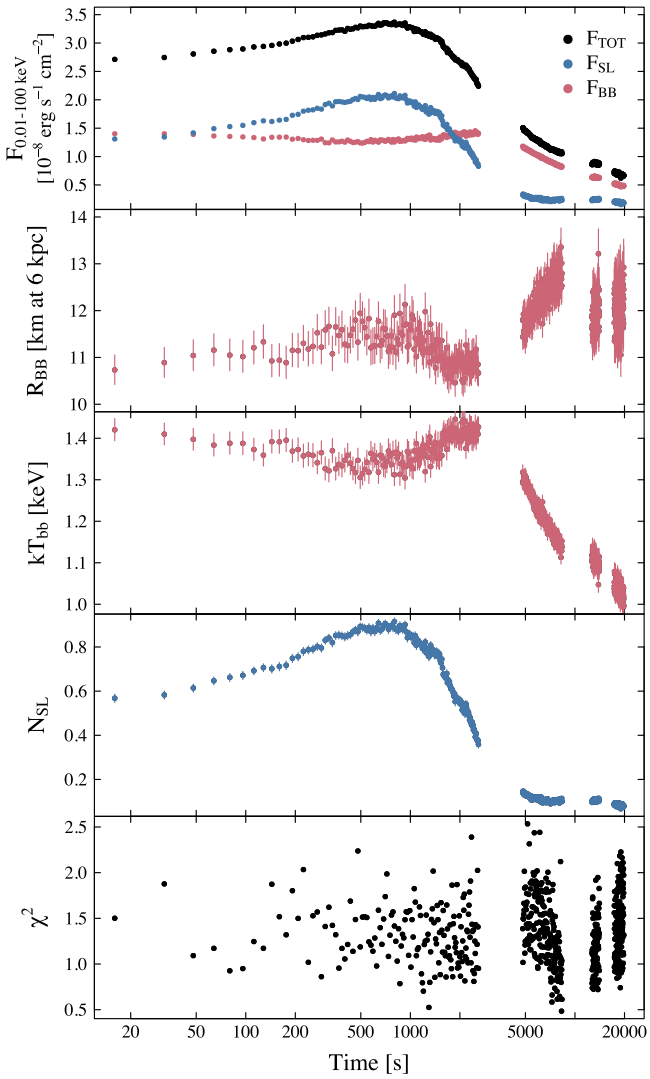

Figure 6. Component fluxes, spectral parameters, and the quality of the spectral fits of the 16 s superburst spectra. From top to bottom: unabsorbed, bolometric (0.1–200 keV) fluxes of the blackbody (BB), Comptonization (SL), and the total (TOT) spectra, the effective radius in kilometers (assuming a distance of 6 kpc) derived from the blackbody normalization, the temperature of the blackbody component, the normalization of the Comptonization component (other parameters are fixed, see the text), and the reduced χ^2 of the spectral fits, respectively.

4. DISCUSSION

Our results indicate that during an X-ray superburst there are at least two variable components: the cooling X-ray burst emission and a quasi-Planckian component with a constant temperature of 2.4–2.6 keV. The fact that the NMF component $k = 1$ (SL) does not break up into several components, and that the spectra can be fitted by imposing a constant temperature (∼2.5 keV) saturated Comptonization model, just as the SL atmosphere calculations by Inogamov & Sunyaev (1999), Suleimanov & Poutanen (2006), Inogamov & Sunyaev (2010) predict, and what is seen in the persistent (accretion) emission in atolls and Z-sources (Gilfanov et al. 2003; Revnivtsev & Gilfanov 2006; Revnivtsev et al. 2013), suggest that a variable SL is present also during the superburst and has a major contribution to the total X-ray spectra. Therefore, our finding provides yet more supporting observational evidence for the SL model in NS–LMXBs.

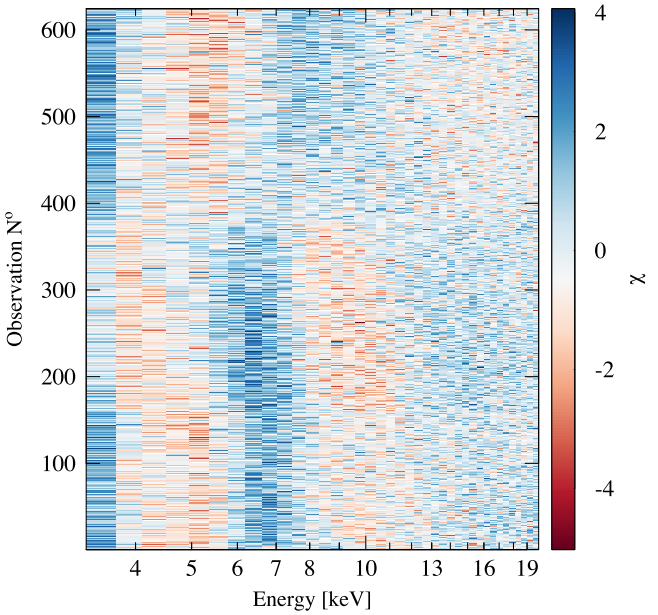

Figure 7. Residuals of the spectral fits shown in Figure 6. There are indications of iron features in the form of an iron line at ∼6.4 keV and a blend of iron edges around ∼9 keV.

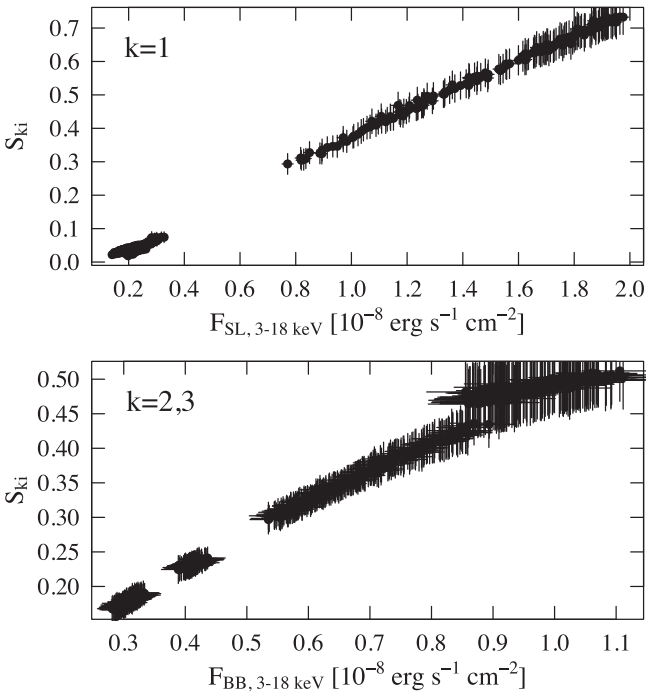

Figure 8. Comparing the spectral component fluxes of the SL and blackbody to their corresponding, averaged NMF signals ($S_{k=1}$, and $S_{k=2,3}$) from all NMF runs. Note that there are deviations from one-to-one correspondence probably due to our use of simple spectral model, component leaking in the NMF decomposition, or the inadequacy of the three component NMF to estimate some (small) spectral features.

Previously, it has been noted that the X-ray burst spectra are statistically much better described if—in addition to a blackbody model describing the burst emission—another variable component is added to the model (in't Zand et al. 2013; Worpel et al. 2013). The first and simplest approach is to model the spectrum prior to the onset of the X-ray burst and allow its flux to vary during the X-ray burst by multiplying the model with a constant (labeled the f_a term). This variable f_a-method was applied to the same superburst data used in this paper by Keek et al. (2014a, 2014b, 2015). We note, however, that none of the individual NMF components could be fitted with the model (CUTOFFPL) that was used to describe the persistent spectrum prior to the X-ray burst in Keek et al. (2014a, 2014b, 2015). Rather, the persistent spectrum can be equally well described by a DISKBB + COMPTT model, where the COMPTT model component takes the same values as during the superburst. We find that the component that changes in normalization (i.e., flux) is the one corresponding to the SL. Thus, the main difference to the previous spectral modeling in Keek et al. (2014a, 2014b, 2015) is that the SL spectrum has more flux at higher energies (above 10 keV) than the cutoff power-law spectrum as fitted to the persistent spectra. For this reason, in our decomposition the burst spectrum appears much cooler during the superburst peak (∼1.4 keV compared to ∼2.5 keV), as the spectrum is now dominated by the SL spectrum at higher energies, but there is a need for more flux in the soft X-rays. Furthermore, our spectral fits result in comparable blackbody radii ranging from ∼11 km in the superburst peak to ∼12 km during the latter three spacecraft orbits, whereas the R_{bb} values during the peak in Keek et al. (2014a) were much lower (∼5 km). These changes may be caused by the SL getting slightly wider, effectively blocking the direct burst emission in the first orbit.

The increase of the persistent emission during X-ray bursts has been interpreted as a momentary increase of the mass accretion rate due to the Poynting–Robertson drag (Walker & Meszaros 1989; Walker 1992; Miller & Lamb 1996). Similarly, during the superburst, one could attribute the increase of the SL emission flux to a 15-fold increase in $\dot{M}$. However, this interpretation suffers from one important drawback. If $\dot{M}$ were to increase by such a large amount, the accretion disc flux should also have increased in concert by the same amount. Assuming that half of the persistent luminosity originates in the accretion disk, the disk flux should contribute a sizable fraction of the total flux during the superburst, in addition to the disk becoming hotter. This is not observed; there is no NMF component (or a sum of components) that can be described by a disk blackbody model (DISKBB) with a variable temperature and a constant normalization that would be expected in this case. An alternative scenario is that the changes in the SL flux are instead caused more directly by the superburst. As speculated in Suleimanov et al. (2011) and Kajava et al. (2014), the X-ray burst occurring underneath the SL can provide additional radiation pressure support to the SL that is "levitating" above the stellar photosphere (Suleimanov & Poutanen 2006). As the SL is radiation pressure supported, the burst emission may push the SL toward higher latitudes during the burst, increasing its luminosity as more burst photons are reprocessed in it, thus mimicking an increase in the accretion rate.

In a recent work by Degenaar et al. (2016) a similar NMF analysis as performed in this paper showed that the persistent spectrum changes during an X-ray burst in the hard state as well. As the burst occurred in the hard state, the SL is likely optically thin and joins smoothly to the optically thin accretion flow, which can be described by a power-law spectral model. The slope of the power-law component changed during the

burst, which is likely caused by a decrease of the equilibrium electron temperature in the hot flow when the external photons from the X-ray burst enter the corona (Ji et al. 2015). This is similar to the black hole X-ray binaries in the case where a variable amount of external disc photons may enter the hot flow in the hard state (Malzac & Belmont 2009; Poutanen & Vurm 2009). It seems therefore that the NMF technique has now revealed two possible physical origins for persistent spectral changes during X-ray bursts: variable electron temperatures during the hard state bursts and a burst induced increase of the SL emission in the soft state bursts.

It remains to be studied whether the superburst from 4U 1820–303—and also normal type-I X-ray bursts—behave the same way as the 4U 1636–536 superburst. However, type-I X-ray bursts cool on much shorter timescales, which reduces the number of good quality spectra per burst, thus making the NMF decomposition not as robust as is the case with a superburst.

5. CONCLUSIONS

Spectral degeneracy, i.e., the ability to fit a variety of models to the same spectrum with comparable quality, is a real problem in X-ray astronomy, which arises either from photon-starved spectra in faint sources and/or smooth and curved spectra in bright sources. A particularly good example can be found in NS–LMXBs, where the spectrum during an X-ray burst and/or soft state consists of multiple blackbody (-like) components with varying temperatures. This ambiguity has led to different interpretations of the constituent spectral components depending on the fit results. We have shown that by using non-negative matrix factorization, the superburst spectra of 4U 1636-536 can be decomposed into two variable spectral components: the cooling burst spectrum and a boundary/spreading layer, which is found to contribute a sizable fraction of the total luminosity during the superburst. The spectral properties of the boundary/spreading layer component favors the spreading layer model (Inogamov & Sunyaev 1999, 2010; Suleimanov & Poutanen 2006), where the spectrum is a constant ∼2.5 keV, quasi-Planckian component varying just in normalization as the burst evolves. This component is also very reminiscent of the frequency-resolved spectral component of a constant spectral shape that is responsible for the sub-second variability in many NS–LMXBs. Smoothly evolving emission from the spreading layer naturally explains the light curves and spectral evolution of the superburst, without the need to invoke a sudden increase of the mass accretion rate (with the Poynting–Robertson mechanism).

We thank Valery Suleimanov, Juri Poutanen, and Guobao Zhang for useful discussions. KIIK and JJEK acknowledge support from the Faculty of the European Space Astronomy Centre (ESAC). JJEK acknowledges support from the ESA research fellowship programme.

REFERENCES

Ballantyne, D. R. 2004, MNRAS, 351, 57
Brunet, J.-P., Tamayo, P., Golub, T. R., & Mesirov, J. P. 2004, PNAS, 101, 4164
Cornelisse, R., Heise, J., Kuulkers, E., Verbunt, F., & in't Zand, J. J. M. 2000, A&A, 357, L21
Cumming, A., & Bildsten, L. 2001, ApJL, 559, L127
Degenaar, N., Koljonen, K. I. I., Chakrabarty, D., et al. 2016, MNRAS, 456, 4256
Deufel, B., Dullemond, C. P., & Spruit, H. C. 2001, A&A, 377, 955
Done, C., Gierliński, M., & Kubota, A. 2007, A&ARv, 15, 1
Galloway, D. K., Psaltis, D., Muno, M. P., & Chakrabarty, D. 2006, ApJ, 639, 1033
Gaujoux, R., & Seoighe, C. 2010, BMC Bioinformatics, 11, 367
Gilfanov, M., Revnivtsev, M., & Molkov, S. 2003, A&A, 410, 217
Grebenev, S. A., & Sunyaev, R. A. 2002, AstL, 28, 150
Houck, J. C., & Denicola, L. A. 2000, in ASP Conf. Ser. 216, Astronomical Data Analysis Software and Systems IX, ed. N. Manset, C. Veillet, & D. Crabtree (San Francisco, CA: ASP), 591
Inogamov, N. A., & Sunyaev, R. A. 1999, AstL, 25, 269
Inogamov, N. A., & Sunyaev, R. A. 2010, AstL, 36, 848
in't Zand, J. J. M., Galloway, D. K., Marshall, H. L., et al. 2013, A&A, 553, A83
Jahoda, K., Markwardt, C. B., Radeva, Y., et al. 2006, ApJS, 163, 401
Ji, L., Zhang, S., Chen, Y., et al. 2015, ApJ, 806, 89
Kajava, J. J. E., Nättilä, J., Latvala, O.-M., et al. 2014, MNRAS, 445, 4218
Keek, L., Ballantyne, D. R., Kuulkers, E., & Strohmayer, T. E. 2014a, ApJ, 789, 121
Keek, L., Ballantyne, D. R., Kuulkers, E., & Strohmayer, T. E. 2014b, ApJL, 797, L23
Keek, L., Cumming, A., Wolf, Z., et al. 2015, MNRAS, 454, 3559
Koljonen, K. I. I. 2015, MNRAS, 447, 2981
Koljonen, K. I. I., McCollough, M. L., Hannikainen, D. C., & Droulans, R. 2013, MNRAS, 429, 1173
Lee, D. D., & Seung, H. S. 1999, Nature, 401, 788
Lee, D. D., & Seung, H. S. 2001, in Advances in Neural Information Processing Systems 13, ed. T. K. Leen, T. G. Dietterich, & V. Tresp (Cambridge, MA: MIT Press)
Lewin, W. H. G., van Paradijs, J., & Taam, R. E. 1993, SSRv, 62, 223
Lin, D., Remillard, R. A., & Homan, J. 2007, ApJ, 667, 1073
Malzac, J., & Belmont, R. 2009, MNRAS, 392, 570
Malzac, J., Petrucci, P. O., Jourdain, E., et al. 2006, A&A, 448, 1125
Meyer, F., Liu, B. F., & Meyer-Hofmeister, E. 2007, A&A, 463, 1
Miller, M. C., & Lamb, F. K. 1996, ApJ, 470, 1033
Mitsuda, K., Inoue, H., Koyama, K., et al. 1984, PASJ, 36, 741
Paatero, P., & Tapper, U. 1994, Environmetrics, 5, 111
Pandel, D., Kaaret, P., & Corbel, S. 2008, ApJ, 688, 1288
Parker, M. L., Fabian, A. C., Matt, G., et al. 2015, MNRAS, 447, 72
Popham, R., & Sunyaev, R. 2001, ApJ, 547, 355
Poutanen, J., & Vurm, I. 2009, ApJL, 690, L97
Pringle, J. E. 1977, MNRAS, 178, 195
Revnivtsev, M. G., & Gilfanov, M. R. 2006, A&A, 453, 253
Revnivtsev, M. G., Suleimanov, V. F., & Poutanen, J. 2013, MNRAS, 434, 2355
Strohmayer, T. E., & Brown, E. F. 2002, ApJ, 566, 1045
Strohmayer, T. E., & Markwardt, C. B. 2002, ApJ, 577, 337
Suleimanov, V., & Poutanen, J. 2006, MNRAS, 369, 2036
Suleimanov, V., Poutanen, J., Revnivtsev, M., & Werner, K. 2011, ApJ, 742, 122
Sunyaev, R. A., & Shakura, N. I. 1986, SvAL, 12, 117
Tauris, T. M., & van den Heuvel, E. P. J. 2006, in Formation and Evolution of Compact Stellar X-ray Sources, ed. W. H. G. Lewin & M. van der Klis (Cambridge: Cambridge Univ. Press)
Titarchuk, L. 1994, ApJ, 434, 570
Vaughan, S., & Fabian, A. C. 2004, MNRAS, 348, 1415
Walker, M. A. 1992, ApJ, 385, 642
Walker, M. A., & Meszaros, P. 1989, ApJ, 346, 844
Worpel, H., Galloway, D. K., & Price, D. J. 2013, ApJ, 772, 94